






Surface termination effect of SrTiO₃ substrate on ultrathin SrRuO₃

Huiyu Wang ¹, Zhen Wang,^{1,2,3,*} Zeeshan Ali ², Enling Wang,⁴ Mohammad Saghayezhian ², Jiandong Guo,⁴ Yimei Zhu,^{3,†} Jing Tao ¹ and Jiandi Zhang ^{4,2,‡}

¹Department of Physics, University of Science and Technology of China, Hefei, Anhui 230026, People's Republic of China

²Department of Physics & Astronomy, Louisiana State University, Baton Rouge, Louisiana 70803, USA

³Department of Condensed Matter Physics & Materials Science, Brookhaven National Laboratory, Upton, New York 11973, USA

⁴Beijing National Laboratory for Condensed Matter Physics, Institute of Physics, Chinese Academy of Sciences, Beijing 100190, People's Republic of China



(Received 3 November 2023; accepted 21 December 2023; published 23 January 2024)

A uniform 1-unit-cell-high step on the SrTiO₃ (STO) substrate is a prerequisite for growing high-quality epitaxial oxide heterostructures. However, it is inevitable that defects induced by mixed substrate-surface termination exist at the interface, significantly impacting the properties of ultrathin films. In this study, we microscopically identify the origin for the lateral inhomogeneity in the growth of ultrathin SrRuO₃ films due to the step effects of SrTiO₃ (001). By using atomic-resolved scanning transmission electron microscopy, we observe two distinct types of step propagation along the [011] and [0 $\bar{1}$ 1] crystallographic direction in SrTiO₃–SrRuO₃ heterostructures, respectively. In particular, the type-II [0 $\bar{1}$ 1] step results in lateral discontinuity of monolayer SrRuO₃ and originates from the SrO-terminated regions along the TiO₂-terminated step edge. Such an induced lateral discontinuity should be responsible for the distinct electronic and magnetic properties of monolayer SrRuO₃. Our findings underscore the critical importance of using single-termination STO substrate to achieve high-quality termination-selective films and to unveil the intrinsic properties of epitaxial films in the atomic limit.

DOI: [10.1103/PhysRevMaterials.8.013605](https://doi.org/10.1103/PhysRevMaterials.8.013605)

I. INTRODUCTION

SrTiO₃ (STO) is a popular substrate because of its compatible lattice parameters with many perovskite oxides. It is the most commonly used substrate for the growth of functional materials, such as high-temperature superconducting, colossal magnetoresistive, and multiferroic films [1–4]. A distinctive characteristic of the STO substrate is the atomic control of a terracelike structure on its surface after chemical and thermal treatment [5–7]. The morphology of substrate-surface step is a sensitive factor that affects the film growth, microstructures, and consequently physical properties. First, uniform unit-cell height steps on the substrate can effectively prevent the formation of three-dimensional islands during film growth, which is beneficial and a prerequisite for realizing high-quality epitaxial films [8,9]. Second, vicinal STO substrates can be used to manipulate film properties by introducing defective structures in thick films, such as antiphase domains [10], out-of-phase domains [11], and stacking faults [12], by taking advantage of step-induced out-of-plane lattice mismatch, structural domain variants regulated by terrace facets [13], and dislocations by providing preferential nucleation sites [14]. These defective structures can lead to ferroelectric and ferromagnetic domains, and act as flux and free-electron pinning centers

[11,15]. Third, steps on the STO substrate have a profound effect on the physical properties of interfaces and ultrathin films. Surface measurements indicate that the presence of steps can lead to an uneven distribution of electrostatic potential [16], which will inevitably lead to inhomogeneity of crystal structure and electronic structure at interfaces and within ultrathin films. For instance, steps induced resistivity anisotropy in LAO/STO [17], which can be attributed to a deteriorative effect on the conductive properties of interfaces [18]. Therefore, revealing the impact of steps and terraces on the atomic and electronic structures of interfaces and ultrathin films is essential for understanding their structure-property relationships.

Current research primarily relies on surface measurements to explore ultrathin film properties and to deduce possible structural and electronic reconstructions that occur at the steps. However, detailed atomic-scale studies of step-induced microstructures using scanning transmission electron microscopy (STEM) are lacking. The main challenge is pinpointing the location of steps at the substrate-film interface and tracking step propagation within the grown film. Two factors make this challenging: first, substrate steps do not introduce obvious structural defects in ultrathin films, such as domains and dislocations. Second, the STEM sample must be cut perpendicular to the step, as any overlap in the projected direction will blur the precise position of the step. Here in this work, we address this challenge and focus on studying the step-induced microstructures in ultrathin SrRuO₃ (SRO) superlattices grown on STO substrate.

*wangzhen03@ustc.edu.cn

†zhu@bnl.gov

‡jiandiz@iphy.ac.cn

Bulk 4d transition-metal oxide SRO exhibits a ferromagnetic (FM)-metallic ground state with a Curie temperature $T_C \sim 160$ K [19]. The metal-insulator transition (MIT) in SRO thin films has been reported at a critical thickness ranging from 4–5 unit cells (u.c.) to 2 u.c. [20–24]. The thickness-dependent MIT transition is attributed to factors such as enhanced electronic correlations [19–21], structural transition [25], dynamic spin correlations [26] and extrinsic effects such as surface disorder and nonstoichiometry [22,23]. Moreover, the ground states of monolayer SRO superlattices, which remove the surface disorder effect, are obtained from a non-FM insulator [23,24] to an FM insulator [27] to borderline FM metal [28]. Notably, these experimental results contradict the theoretically proposed FM half-metallic state for monolayer SRO confined within the STO lattice [20]. Excluding extrinsic factors will help us to address the inconsistencies between experimental and theoretical results and uncover the intrinsic properties of monolayer SRO. One crucial question is whether the commonly observed substrate-surface steps result in defects in monolayer SRO. In addition, how the step propagates in the SRO film, which would provide direct evidence for the film growth mode, remains unclear thus far.

To address these questions, we studied the step-induced microstructures in $\text{STO}^5\text{-SRO}^2\text{-STO}^5\text{-SRO}^1$ heterostructure grown on a vicinal STO (001) substrate using atomic-resolved STEM and electron-energy-loss spectroscopy (EELS). Unlike atomic force microscopy (AFM) and scanning tunneling microscopy (STM), which are commonly utilized to investigate the SRO growth process through the surface morphology, our STEM observations directly provide atomic structure information in the cross-sectional view of the interface and film. We observed two types of step propagation modes in the film specifically along the [011] and $[0\bar{1}1]$ crystallographic directions, which have distinct effects on the lateral homogeneity of the SRO layers. The step propagation mode is found to be related to the SrO-terminated region along the step edge. Our findings provide further insight into the mechanism underlying the physical properties of interfaces and ultrathin films.

II. METHODS

A. Film growth and surface characterization

Heterostructures of $\text{STO}^5\text{-SRO}^2\text{-STO}^5\text{-SRO}^1$ and $\text{STO}^5\text{-SRO}^3\text{-STO}^5\text{-SRO}^1$ were fabricated via pulsed-laser deposition on TiO_2 -terminated STO (001) substrates. The STO substrates were first sonicated in deionized water and then treated for 30 s in buffered hydrogen fluoride (BHF), and finally annealed at 950°C in an oxygen atmosphere to generate atomically smooth surfaces [29]. The TiO_2 -terminated STO (001) substrate is atomically smooth with steps of 1 u.c. in height. The SRO and STO films were grown at 650°C with oxygen pressures of 100 and 10 mTorr, respectively. A KrF excimer laser ($\lambda = 248$ nm) repetition with a rate of 10 Hz (SRO) and 5 Hz (STO), and energy of 300 mJ (SRO) and 260 mJ (STO) was used. After deposition, the samples were cooled at $\sim 12^\circ/\text{min}$ to room temperature in 100-mTorr oxygen. The surfaces of the substrates were characterized using AFM. The film thickness

was monitored by *in situ* reflection high-energy electron diffraction.

B. Composition and structural characterization

TEM samples were prepared using a focused ion beam with Ga^+ ions followed by Ar^+ ion milling to a thickness of ~ 30 nm. These TEM samples were cut in the direction perpendicular to the steps to ensure that the probing electron beam was parallel to the step edge without atom overlap. STEM and EELS experiments were conducted using a 200-kV JEOL ARM electron microscope equipped with double-aberration correctors, a dual energy-loss spectrometer, and a cold field-emission source. The atomic-resolution high-angle annular dark-field (HAADF) STEM image was collected with a 21-mrad convergent angle and a collection angle of 67–275 mrad. The microscope conditions were optimized for EELS acquisition with a probe size of 0.8 \AA , a convergence semi-angle of 20 mrad, and a collection semiangle of 88 mrad. EELS mapping was obtained across the whole film with a step size of 0.2 \AA and a dwell time of 0.05 s per pixel. The EELS background was subtracted using a power-law function, and the multiple-scattering effect was removed with a Fourier deconvolution method.

III. RESULTS

A. Atomic structure of $\text{STO}^5\text{-SRO}^n\text{-STO}^5$ ($n = 1, 2$) heterostructures

Bulk SRO crystallizes in an orthorhombic structure with space group $Pbnm$ (No. 62) and a tilt pattern of $a^-a^-c^+$ at room temperature. The SRO grown on a TiO_2 -terminated STO substrate undergoes a 0.5% compressive strain (bulk: $a_{\text{STO}} = 3.905 \text{ \AA}$ and $a_{\text{pSRO}} = 3.925 \text{ \AA}$). The atomic structure of the $\text{STO}^5\text{-SRO}^n\text{-STO}^5$ ($n = 1, 2$) heterostructures on atomically flat region of the STO substrate was thoroughly investigated in our previous work [23]. Electric and magnetotransport measurements demonstrate that $\text{STO}^5\text{-SRO}^1\text{-STO}^5$ is insulating and non-FM, whereas $\text{STO}^5\text{-SRO}^2\text{-STO}^5$ is FM metallic with a Curie temperature of ~ 128 K. The SRO-STO heterostructures are fully strained to the STO substrate; hence, the SRO layers exhibit slightly increased out-of-plane lattice parameters compared to the value for bulk SRO. Due to connectivity with TiO_6 octahedra in cubic STO, the ultrathin 2-u.c. and monolayer SRO display tetragonal symmetry without RuO_6 tilt. Therefore, the $\text{STO}^5\text{-SRO}^n\text{-STO}^5$ heterostructures provide an ideal platform, without defects such as dislocations and out-of-phase domains, for studying substrate-surface step propagation and its effect on the microstructures of heterostructures.

B. Two types of steps

Throughout the entire film, the substrate step terraces are on a micrometer scale, similar to the AFM observations mentioned later. However, in order to microscopically reveal the step effects on SRO layers, we carefully searched for the region with bunched steps. Figure 1 displays the HAADF-STEM images from two representative

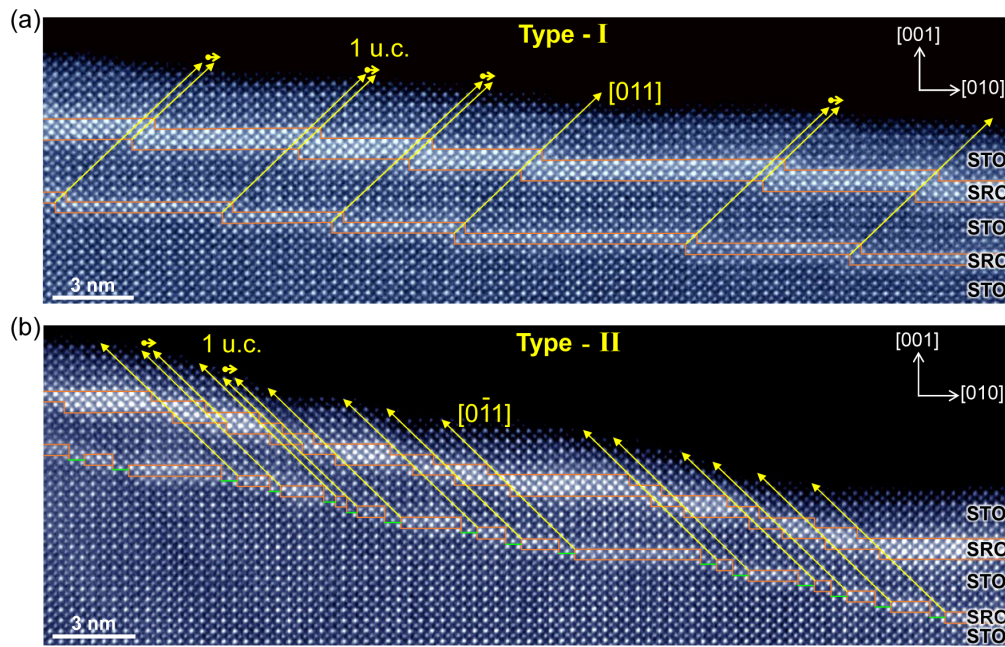


FIG. 1. Cross-sectional STEM image of a STO⁵–SRO²–STO⁵–SRO¹ heterostructure on (001) STO substrate taken along the [100] direction, displaying two propagation modes of the 1-u.c.-height step within the heterostructure. (a) Type-I step propagating along the [011] direction from the upper toward lower terrace. (b) Type-II step spreading in the [0 $\bar{1}$ 1] direction from the lower to upper terrace. The orange lines mark TiO₂–SrO interfaces between substrate heterostructure and SRO-STO layers in the heterostructure, while the green lines hereinafter mark the SrO-terminated regions along the substrate step edges. Yellow arrows indicate the step propagation direction in the heterostructure. The 1-u.c. deviation in step propagation toward lower terrace is denoted by short yellow arrows.

step-propagating paths in the STO⁵–SRO²–STO⁵–SRO¹ heterostructures. The intensity in the HAADF image is proportional to the atomic number ($Z^{2/1.7}$), and thus allows distinguishing the Ru ($Z = 44$), Sr ($Z = 38$), and Ti ($Z = 22$) columns in the images. The SRO-STO interfaces, marked by orange lines, highlight the step positions, allowing us to track step propagation within the heterostructure, which is not attainable in pure film. Terraces on the STO substrate surface, indicated by orange lines, are 1 u.c. in height and range in width from 1 to 5 nm. Figure 1(a) presents steps propagating in the [011] direction from the higher terrace toward the lower terrace, referred to as type-I step, which is predominant in the film. As the film grows, the type-I step moves forward 1 u.c. in the upper layer with respect to the lower layer, leading to the propagation of the [011] direction. Some type-I steps proceed an extra 1 u.c. along the [010] direction, making the propagation slightly deviate from the [011] direction, as illustrated by arrows in Fig. 1(a). Figure 1(b) shows a type-II step that moves in the [0 $\bar{1}$ 1] direction from the lower to upper terrace. In contrast to the type-I step, the type-II step moves backward 1 u.c. in the upper layer during the film growth process, resulting in propagation along the [0 $\bar{1}$ 1] direction. Some type-II steps proceed one fewer unit cell in the [0 $\bar{1}$ 0] direction, making the propagation slightly deviate from the [0 $\bar{1}$ 1] direction.

We performed STEM-EELS mapping to study the elemental distribution in the heterostructure. Figure 2 displays Ti elemental map across the STO⁵–SRO²–STO⁵–SRO¹ heterostructure, in which the SRO layers start with SrO layers and terminate with RuO₂ layers. The bottom SRO layer is

1-u.c. thick, and approximately 30% of Ru is doped into the TiO₂–terminated layer of STO substrate. As indicated by the arrows in Fig. 2(b), the Ti columns show darker intensities in the elemental map and higher intensities in the Z-contrast HAADF image [see Fig. 2(a)], indicating the presence of Ru dopants in these Ti columns. In addition, the Ru columns at step edges exhibit lower intensities in the HAADF image of Fig. 2(a), suggesting Ti diffusion into the Ru columns.

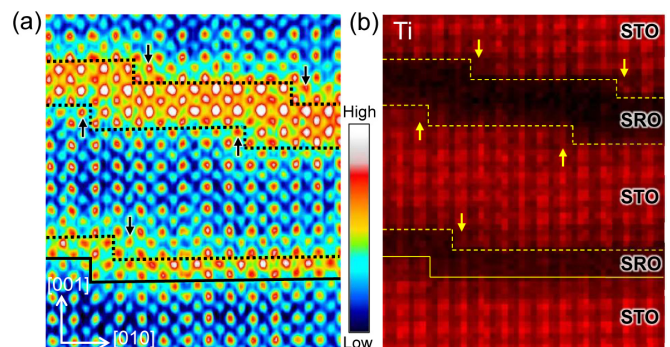


FIG. 2. Chemical intermixing at the step edges in STO⁵–SRO²–STO⁵–SRO¹ observed by STEM-EELS. (a) False-color HAADF image and (b) corresponding EELS elemental map extracted from Ti *L* edge. Solid orange lines denote the substrate-heterostructure interface, highlighting 1-u.c.-height step on substrate surface. Dashed orange lines mark the TiO₂–SrO interfaces, highlighting step locations within the heterostructure. Arrows indicate Ti columns with Ru dopants at the step edges.

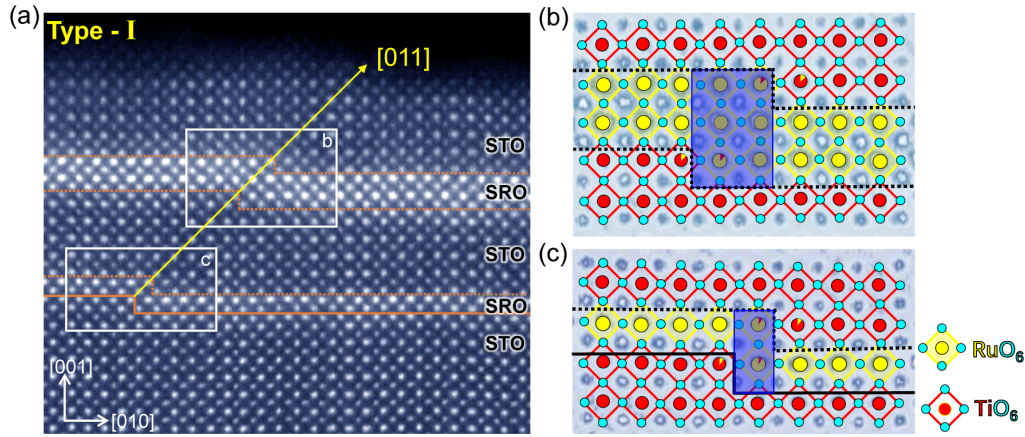


FIG. 3. Atomic arrangement of the type-I step in $\text{STO}^5\text{-SRO}^2\text{-STO}^5\text{-SRO}^1$. (a) HAADF image of the type-I step. Enlarged view of steps in the (b) top 2-u.c. and (c) bottom 1-u.c. SRO layers sandwiched by STO. Crystal structure models are superimposed. The Ru-Ti intermixing is indicated by the yellow Ru atoms with fractional occupation of Ti atoms (red), which is estimated from the intensity in the HAADF image. The STO substrate-heterostructure interface and $\text{TiO}_2\text{-SrO}$ of STO and SRO layers are denoted by solid and dashed orange lines, respectively. Blue rectangles highlight the inhomogeneous blocks in SRO layers between the steps.

Such Ti-Ru intermixing primarily occurs within a unit cell located at the step edge. This observation indicates that the heterostructure prefers to grow from the step edge, even employing the layer-by-layer growth mode [23]. It provides direct evidence that the step edges are preferential nucleation sites because of more coordination [9]. The EELS elemental mapping is consistent with the HAADF observations, demonstrating that the intensity of the Z-contrast HAADF image allows us to locate the steps and Ru-Ti intermixing columns in examining the atomic structure of the steps described below.

C. Step effect on the sandwiched ultrathin SRO heterostructures

Detailed analysis of atomic-resolved HAADF-STEM images (Figs. 3 and 4) reveals that these two types of steps induce lateral inhomogeneity within the heterostructure and affect

the thickness of the SRO layers in opposite ways. The type-I $[011]$ step moves forward in the subsequent layer, adding an extra unit cell to the SRO layers in the film growth direction between the step edges [see Fig. 3(a)]. As indicated by the blue rectangle depicted in Figs. 3(b) and 3(c), the top 2-u.c. SRO layers contain a 3-u.c. block while the bottom 1-u.c. SRO layer has a 2-u.c. block. The block in the 3-u.c. SRO layers, located between the step edges, changed to 4 u.c. in the $\text{STO}^5\text{-SRO}^3\text{-STO}^5\text{-SRO}^1$ heterostructure (see Fig. 9 in Appendix A), exhibiting the same tendency. On the other hand, the type-II $[0\bar{1}1]$ step removes a SRO unit cell between the steps in the $[001]$ direction as it moves backward in the subsequent layer. Figure 4 shows the top 2-u.c. SRO layers reduced to 1 u.c. in the block, and the bottom 1-u.c. SRO layer became discontinuous. Furthermore, Ti-Ru intermixing was observed at the step edges of STO-SRO interfaces.

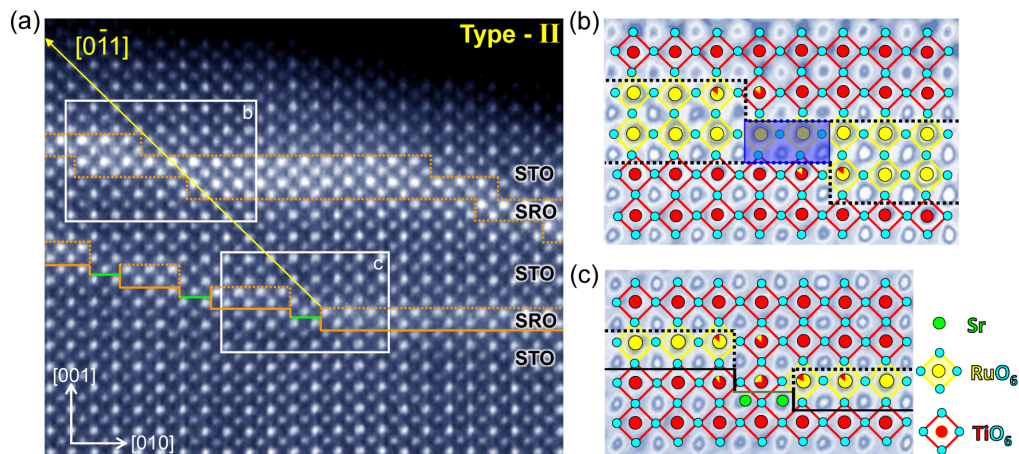


FIG. 4. Structure feature of the type-II step in $\text{STO}^5\text{-SRO}^2\text{-STO}^5\text{-SRO}^1$. (a) HAADF image of the type-II step. Enlarged image of steps in the (b) top 2-u.c. and (c) bottom 1-u.c. SRO layers from the rectangles in (a). Projected crystal structures are superimposed. Solid lines indicate the substrate-heterostructure interface, with SrO-terminated region highlighted by green lines. The dashed lines mark the $\text{TiO}_2\text{-SRO}$ interfaces between the STO and SRO layers. Blue rectangles highlight the SRO blocks.

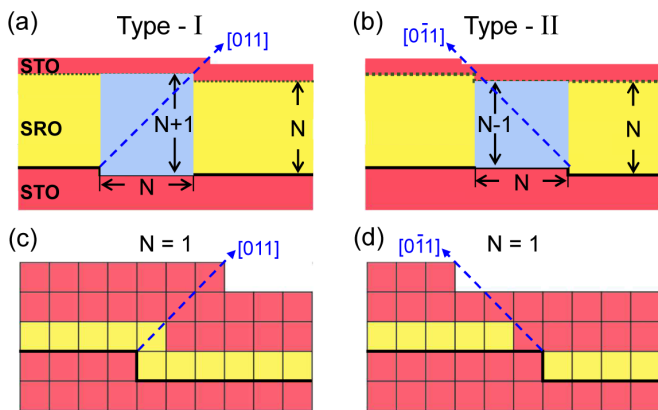


FIG. 5. Schematic illustration of formation process of the (a) type-I and (b) type-II steps on STO substrate with 1-u.c.-height step. “N” denotes the thickness of SRO layers in unit cells. The monolayer SRO with $N = 1$ in (c) type-I and (d) type-II steps.

Figure 5 schematically illustrates the structural features of these two types of steps in the STO-SRO heterostructure on the STO substrate with 1-u.c.-height steps. Within the region where the step passes through, the N -u.c. SRO layers change in thickness. For the type-I step which shifts along the $[110]$ direction, it forms an $N \times (N + 1)$ block at the step edge for N -u.c. SRO layers [see Fig. 5(a)]. On the other hand, the $[0\bar{1}1]$ propagating type-II step introduces an $N \times (N - 1)$ block at the step edge for $N - 1$ u.c. SRO layers [see Fig. 5(b)]. When the SRO layer is reduced to 1 u.c. ($N = 1$), the type-I step can still maintain the continuous connection for the single-u.c. SRO layer [see Fig. 5(c)], while the type-II step destroys the in-plane continuity of the SRO layer [see Fig. 5(d)], which would be expected to significantly affect the transport property of the monolayer SRO.

IV. DISCUSSION

A. Origin of the type-II $[0\bar{1}1]$ step

Since the type-II step causes discontinuities of monolayer SRO, its formation mechanism needs to be investigated. Our

STEM observations reveal the presence of both types of steps in different regions throughout the entire film, irrespective of the terrace width on the substrate, suggesting no direct correlation between the step type and terrace width. As illustrated in Fig. 5, the step type is primarily determined by the initial grown layer interfacing with the substrate, as the subsequent layer exhibits the same step feature as the preceding layer in the film growth process. For the $[011]$ propagating type-I step, the first SRO layer mimics the substrate step feature, which should be energetically favorable, and hence, the type-I step was commonly observed experimentally. In contrast, the initial grown layer of the $[0\bar{1}1]$ propagating type-II step leaves behind an uncovered unit cell at the step edge on the substrate [see Figs. 4, 5(b), and 5(d)], where the substrate is terminated with SrO layer and encounters a half-u.c. step case, thus suggesting that SRO prefers to grow on the TiO_2 -rather than SrO-terminated layer [30]. Regrettably, in STEM images, it is not possible to discern the 1-u.c.-width SrO-terminated region on the substrate following the growth of the STO layer. However, a wider SrO-terminated region can be observed since it introduces vacancies in the STO layer.

HAADF images in Fig. 6 show a type-II step on the STO substrate with a 4-u.c.-width SrO-terminated region along the step edge. The SRO layers become discontinuous above the SrO-terminated region. Specifically, the top SRO layers [see Fig. 6(b)] appear partially discontinuous because most Ru atoms are replaced by Ti in the 1-u.c. block. The bottom single-u.c. SRO layer is completely disconnected in the SrO-terminated region [see Fig. 6(c)], which is filled with STO. In addition, the darker intensity observed above the SrO-terminated region compared to the other parts of the film is caused by the presence of randomly distributed vacancies of O as well as Sr and Ti within STO [see Figs. 6(a) and 6(c)]. The observation indicates that during film growth process, the subsequent STO does not entirely fill the area above the SrO-terminated region. The 1-u.c.-height step propagates in the $[0\bar{1}1]$ direction with respect to the lower terrace edge on the STO substrate. The region of thickness reduction extends to 3 u.c. in the top SRO layers, which is affected by both the thickness of SRO layers and the width of

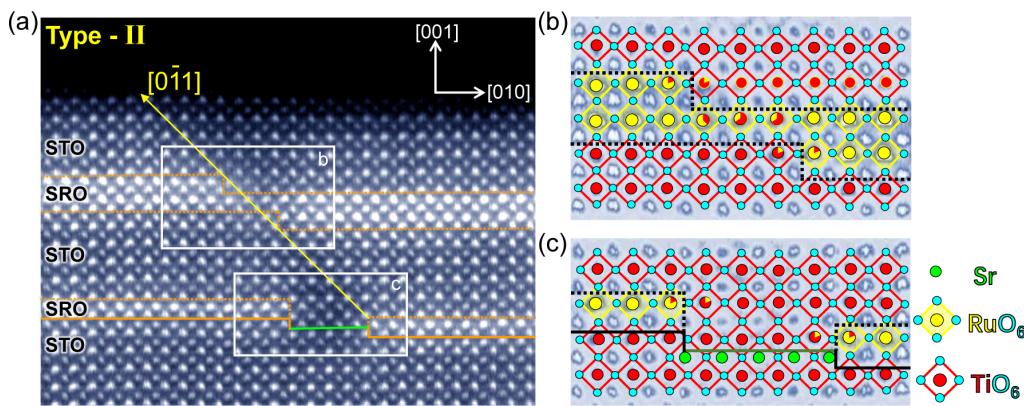


FIG. 6. Atomic structure of type-II step in $\text{STO}^5\text{-SRO}^2\text{-STO}^5\text{-SRO}^1$ on STO substrate with 4-u.c.-width SrO-terminated region along step edge. (a) HAADF image showing the step propagating in the $[0\bar{1}1]$ direction. Enlarged image of steps in the (b) top 2-u.c. SRO and (c) bottom 1-u.c. SRO layers sandwiched by STO. The solid line marks the substrate-heterostructure interface, including 4-u.c.-width SrO-terminated region highlighted by green line. The dark intensity above non-SRO covered SrO-terminated region is caused by the presence of vacancies of O, Sr, and Ti.

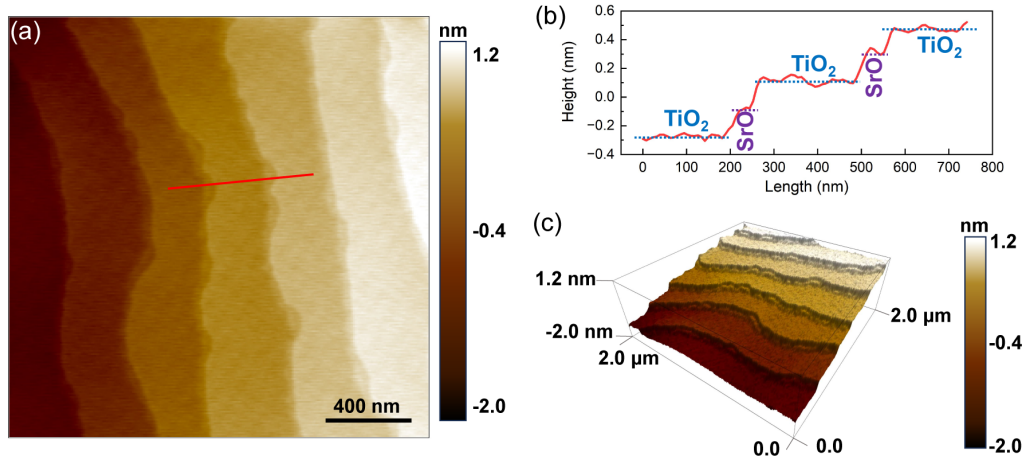


FIG. 7. (a) A typical AFM image of STO substrate with large TiO_2 -terminated surface. (b) A line profile [marked as the red line in (a)]. (c) The corresponding 3D view of the STO surface displayed in (a).

the SrO-terminated region on the substrate (see Fig. 10 in Appendix B).

B. Step effect on physical properties

Before discussing the effect of steps on physical properties, it is crucial to address the following question: Is the SrO-terminated region decorated at step edges a common feature on the TiO_2 -terminated STO substrate? BHF solution etching for 30 s in our case is proposed to be the optimal condition for removing the SrO-terminated region along the step, while a longer etching time would result in the formation of holes on the substrate [29]. Unfortunately, the optimal etching time varies depending on the quality of STO substrates [29]. The surface of STO presented in Fig. 7 is typically obtained by sonicating the substrate in deionized water for 30 min, then etching it with BHF for 36 s, and then annealing at 930°C for

half an hour in an oxidizing atmosphere. Figures 7(a) and 7(c) show the surfaces after these treatments. The surface of the STO is composed of steps and atomically flat large terraces. The height between adjacent large terraces is 3.9 \AA , i.e., 1 STO u.c. high. All these large terraces consist of TiO_2 [5], while small terraces located at the edge of the steps are also observed. According to the line profile displayed in Fig. 7(b), these small terraces are 10–20 nm wide and $\sim 2.0 \text{ \AA}$ high, which equals to the height of half STO unit cell. This suggests that these small terraces along the step edges consist of SrO layers.

To see the structural effect of the SrO layer decorated at the steps of TiO_2 -terminated STO surface, we grew a 5-u.c. STO-capped SRO film on STO substrate and examined it with STEM. As shown in Fig. 8, the film is discontinuous above the wider SrO-terminated regions along the step edge of the TiO_2 -terminated surface. The capped STO layers filled the

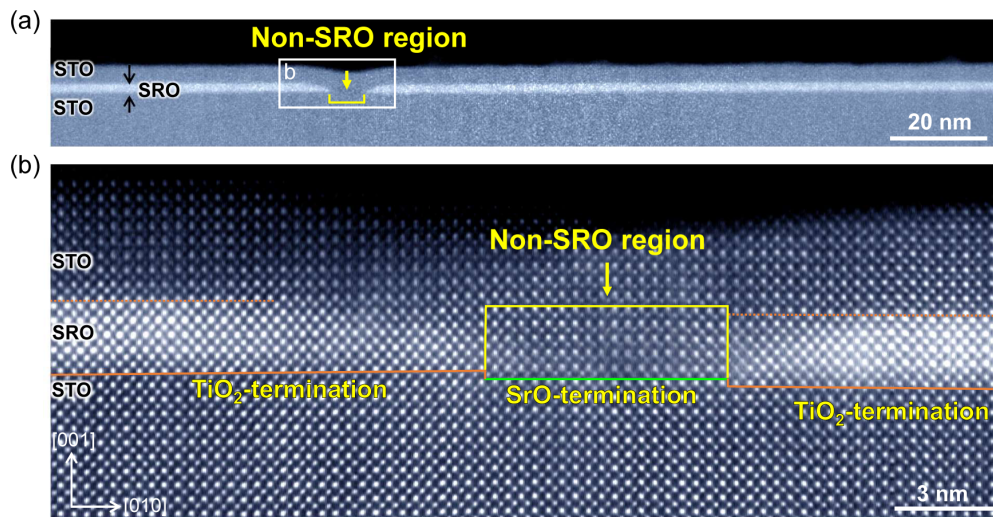


FIG. 8. Discontinuous SRO thin film induced by a SrO-terminated region along the 1-u.c.-height step on TiO_2 -terminated STO substrate. (a) Low-magnification HAADF image of STO-capped 5-u.c. SRO film on STO(001) substrate taken along the [100] direction. Black arrows mark SRO film with bright intensity. The yellow arrow signifies a non-SRO region with dark intensity and groove in the capped STO. (b) Atomic-resolved HAADF image from the rectangle region in (a). The substrate-heterostructure interface is indicated by solid orange lines, with a SrO-terminated region at the step edge marked by green line. The non-SRO region was filled with the capped STO.

bare SrO-terminated region, resulting in grooves on the film surface. The groove is wider than the SrO-terminated region on the substrate because the SRO layers grow in opposite directions.

The STO step edges with SrO-decorated regions can also introduce lateral discontinuity (or inhomogeneities due to the replacement of Ru with Ti) in the SRO films and heterostructures. As demonstrated in Fig. 4, the steps with 1-u.c.-width SrO decoration can lead to discontinuity of monolayer SRO. A wider SrO-decorated region would destroy the continuity of a thicker SRO film. Given that conductivity is measured on the grown films, the atomic-level discontinuity, capable of abruptly interrupting the pathway in electric transport, should be taken into account in the understanding of nonmetallic “dead”-layer issue in ultrathin SRO films and superlattices. It is worth noting that wider SrO-terminated regions along the step edges on the STO surface can be identified from the low-magnification AFM or STM images, but the unit-cell-width SrO-terminated region cannot be distinguished unambiguously.

Single TiO₂-terminated STO substrate at atomic level is a mandatory condition to achieve high-quality termination-selective ultrathin films and to reveal their physical properties. The aforementioned SRO/STO heterostructure is termination selective in the growth process, while the well-known LaAlO₃(LAO)/STO film is indeed termination dependent in the interface properties too. In the LAO/STO(001) case, the LaO-TiO₂ interface exhibits two-dimensional electron gas (2DEG) while the AlO₂-SrO interface is insulating. Excluding the SrO-terminated region at the step edges is

essential to understand the contrary effect of step edges on the 2DEG [25,26], electron phase separation at low temperatures [27], as well as the long-standing dead-layer issue in ultrathin oxide films in general.

V. CONCLUSIONS

In conclusion, the cross-sectional STEM study of the STO⁵-SRO²-STO⁵-SRO¹ heterostructure, grown on a TiO₂-terminated vicinal STO(001) substrate, reveals two distinct step propagation paths. The type-I [011] propagation step moves from the higher to lower terrace, leading to an extra SRO unit cell between the steps in the film growth direction. In contrast, the type-II [0 $\bar{1}$ 1] propagation step removes 1 SRO unit cell in the film growth direction, resulting in the discontinuity of 1-monolayer SRO. Furthermore, SrO-terminated region along the TiO₂-terminated step edge is found to be the origin of the type-II step. A precise depiction of lateral inhomogeneities at the atomic scale would help greatly enhance our grasp of the intrinsic physical properties of ultrathin films, particularly in the case of superlattices.

ACKNOWLEDGMENTS

This work was primarily supported by the U.S. Department of Energy (DOE) under Grant No. DOE DE-SC0002136. The electron microscopic work done at Brookhaven National Laboratory (BNL) was sponsored by the U.S. DOE-BES, Materials Sciences and Engineering Division, under Contract No. DE-SC0012704. Part of this work was supported by the National Key R&D Program of China (Grant No.

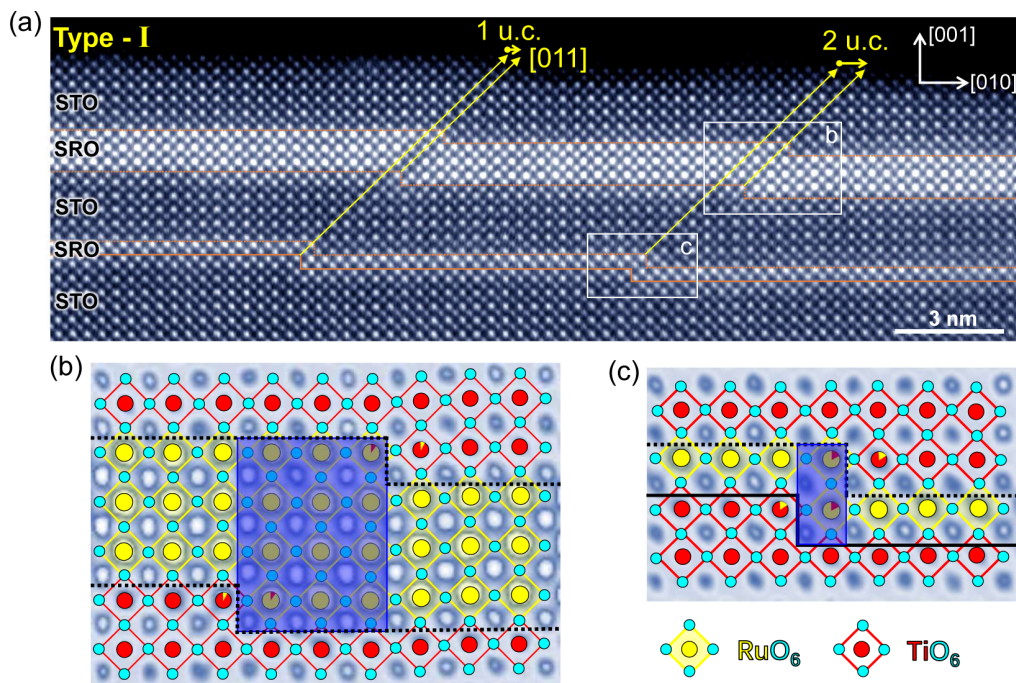


FIG. 9. Structure feature of the type-I step in STO⁵-SRO³-STO⁵-SRO¹ taken along the [100] direction. (a) HAADF image of the type-I step. Enlarged images of steps within the (b) top 3-u.c. and (c) bottom 1-u.c. SRO layers from the rectangles in (a). Projected crystal structures are superimposed. Solid lines indicate the substrate-heterostructure interface. Dashed lines mark the TiO₂-SrO interfaces within STO-SRO heterostructure. Blue rectangles highlight the SRO blocks with changed thickness.

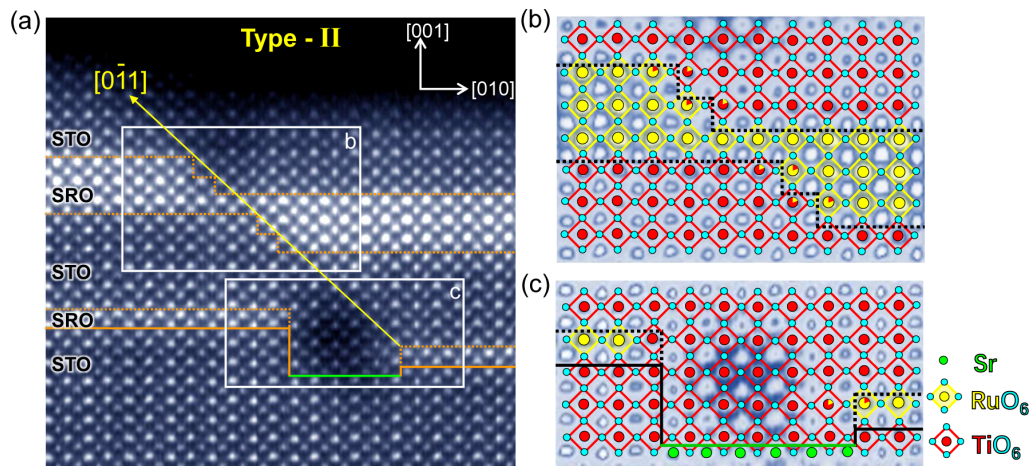


FIG. 10. Type-II step in $\text{STO}^5\text{-SRO}^3\text{-STO}^5\text{-SRO}^1$ heterostructure on the TiO_2 -terminated STO substrate with SrO-terminated region along a 2-u.c.-height step edge. (a) HAADF image showing the step propagation in the $[0\bar{1}1]$ direction. Solid lines indicate the substrate-heterostructure interface. The green line highlights the SrO-terminated region. Enlarged view of the areas indicated by rectangles in (a) showing steps in the (b) top 3-u.c. and (c) bottom 1-u.c. SRO layers. In (c), solid black line marks the STO substrate surface with 5-u.c.-width SrO-terminated region at the step. The dark intensity above the SrO-terminated region is induced by vacancies of O, Sr, and Ti.

2022YFA1403000), the National Natural Science Foundation of China (Grant No. 12304035), and the Strategic Priority Research Program of Chinese Academy of Sciences (Grant No. XDB33000000).

APPENDIX A: ATOMIC STRUCTURE OF THE TYPE-I STEP IN $\text{STO}^5\text{-SRO}^3\text{-STO}^5\text{-SRO}^1$ HETEROSTRUCTURE

Figure 9 displays an HAADF-STEM image of the $\text{STO}^5\text{-SRO}^3\text{-STO}^5\text{-SRO}^1$ heterostructure on the TiO_2 -terminated STO substrate with 1-u.c.-height steps. The step advances in the $[110]$ direction, with 1- or 2-u.c. deviation toward the lower terrace. In the $[001]$ film growth direction, the top 3-u.c. SRO layers changed to 4 u.c. in the block between the step edges, as indicated by the blue rectangle in Fig. 9(b).

APPENDIX B: ATOMIC STRUCTURE OF TYPE-II STEP IN $\text{STO}^5\text{-SRO}^3\text{-STO}^5\text{-SRO}^1$ HETEROSTRUCTURE

Figure 10 displays the type-II step in the $\text{STO}^5\text{-SRO}^3\text{-STO}^5\text{-SRO}^1$ heterostructure. The orange lines highlight a 2-u.c.-height step on the TiO_2 -terminated STO substrate, featuring a 5-u.c.-width SrO-terminated region at the step edge. The 2-u.c.-height step grows in the $[110]$ direction with respect to the lower terrace, as denoted by yellow arrows in Fig. 10(a). The bottom 1-u.c. SRO layer is discontinuous due to the absence of SRO coverage on the SrO-terminated region. The dark intensity above the SrO-terminated region indicates that subsequent growth of STO does not completely fill this region and introduces vacancies of O, Sr, and Ti. The thickness of the top 3-u.c. SRO layers changes to 2 and 1 u.c. between the steps, as illustrated by the crystal structure models in Fig. 10(b).

- [1] B. W. Kang, A. Goyal, D. F. Lee, J. E. Mathis, E. D. Specht, P. M. Martin, D. M. Kroeger, M. Paranthaman, and S. Sathymurthy, Comparative study of thickness dependence of critical current density of $\text{YBa}_2\text{Cu}_3\text{O}_{7-x}$ on (100) SrTiO_3 and on rolling-assisted biaxially textured substrates, *J. Mater. Res.* **17**, 1750 (2002).
- [2] J. J. Lee, F. T. Schmitt, R. G. Moore, S. Johnston, Y.-T. Cui, W. Li, M. Yi, Z. K. Liu, M. Hashimoto, Y. Zhang *et al.*, Interfacial mode coupling as the origin of the enhancement of T_c in FeSe films on SrTiO_3 , *Nature (London)* **515**, 245 (2014).
- [3] Z. Liao, F. Li, P. Gao, L. Li, J. Guo, X. Pan, R. Jin, E. W. Plummer, and J. Zhang, Origin of the metal-insulator transition in ultrathin films of $\text{La}_{2/3}\text{Sr}_{1/3}\text{MnO}_3$, *Phys. Rev. B* **92**, 125123 (2015).
- [4] J. Wang, J. B. Neaton, H. Zheng, V. Nagarajan, S. B. Ogale, B. Liu, D. Viehland, V. Vaithyanathan, D. G. Schlom, U. V. Waghmare *et al.*, Epitaxial BiFeO_3 multiferroic thin film heterostructures, *Science* **299**, 1719 (2003).
- [5] M. Kawasaki, K. Takahashi, T. Maeda, R. Tsuchiya, M. Shinohara, O. Ishiyama, T. Yonezawa, M. Yoshimoto, and H. Koinuma, Atomic control of the SrTiO_3 crystal surface, *Science* **266**, 1540 (1994).
- [6] M. Kareev, S. Prosandeev, J. Liu, C. Gan, A. Kareev, J. W. Freeland, M. Xiao, and J. Chakhalian, Atomic control and characterization of surface defect states of TiO_2 terminated SrTiO_3 single crystals, *Appl. Phys. Lett.* **93**, 061909 (2008).
- [7] J. G. Connell, B. J. Isaac, G. B. Ekanayake, D. R. Strachan, and S. S. A. Seo, Preparation of atomically flat SrTiO_3 surfaces using a deionized-water leaching and thermal annealing procedure, *Appl. Phys. Lett.* **101**, 251607 (2012).
- [8] M. Naito, H. Yamamoto, and H. Sato, Reflection high-energy electron diffraction and atomic force microscopy studies on homoepitaxial growth of $\text{SrTiO}_3(001)$, *Physica C* **305**, 233 (1998).
- [9] H. M. Christen and G. Eres, Recent advances in pulsed-laser deposition of complex oxides, *J. Phys.: Condens. Matter* **20**, 264005 (2008).

- [10] M. A. Zurbuchen, W. Tian, X. Q. Pan, D. Fong, S. K. Streiffer, M. E. Hawley, J. Lettieri, Y. Jia, G. Asayama, S. J. Fulk *et al.*, Morphology, structure, and nucleation of out-of-phase boundaries (OPBs) in epitaxial films of layered oxides, *J. Mater. Res.* **22**, 1439 (2007).
- [11] E. Gradauskaite, K. A. Hunnestad, Q. N. Meier, D. Meier, and M. Trassin, Ferroelectric domain engineering using structural defect ordering, *Chem. Mater.* **34**, 6468 (2022).
- [12] T. Haage, J. Zegenhagen, J. Q. Li, H.-U. Habermeier, M. Cardona, Ch. Jooss, R. Warthmann, A. Forkl, and H. Kronmüller, Transport properties and flux pinning by self-organization in YBa₂Cu₃O_{7-x} films on vicinal SrTiO₃(001), *Phys. Rev. B* **56**, 8404 (1997).
- [13] Q. Gan, R. A. Rao, and C. B. Eom, Control of the growth and domain structure of epitaxial SrRuO₃ thin films by vicinal (001) SrTiO₃ substrates, *Appl. Phys. Lett.* **70**, 1962 (1997).
- [14] J. S. Wu, C. L. Jia, K. Urban, J. H. Hao, and X. X. Xi, Stair-rod dislocations in perovskite films on LaAlO₃ substrates, *Philos. Mag. Lett.* **81**, 375 (2001).
- [15] B. Paudel, B. Zhang, Y. Sharma, K. T. Kang, H. Nakotte, H. Wang, and A. Chen, Anisotropic domains and antiferrodistortive-transition controlled magnetization in epitaxial manganite films on vicinal SrTiO₃ substrates, *Appl. Phys. Lett.* **117**, 081903 (2020).
- [16] Y. Li, J. R. Sun, J. L. Zhao, and B. G. Shen, Surface electronic inhomogeneity of the (001)-SrTiO₃:Nb crystal with a terrace-structured morphology, *J. Appl. Phys.* **114**, 154303 (2013).
- [17] P. Brinks, W. Siemons, J. E. Kleibeuker, G. Koster, G. Rijnders, and M. Huijben, Anisotropic electrical transport properties of a two-dimensional electron gas at SrTiO₃-LaAlO₃ interfaces, *Appl. Phys. Lett.* **98**, 242904 (2011).
- [18] T. Fix, F. Schoofs, Z. Bi, A. Chen, H. Wang, J. L. MacManus-Driscoll, and M. G. Blamire, Influence of SrTiO₃ substrate miscut angle on the transport properties of LaAlO₃/SrTiO₃ interfaces, *Appl. Phys. Lett.* **99**, 022103 (2011).
- [19] M. Meng, Z. Wang, A. Fathima, S. Ghosh, M. Saghayezhian, J. Taylor, R. Y. Jin, Y. Zhu, S. T. Pantelides, J. D. Zhang *et al.*, Interface-induced magnetic polar metal phase in complex oxides, *Nat. Commun.* **10**, 5248 (2019).
- [20] M. Verissimo-Alves, P. García-Fernández, D. I. Bilc, P. Ghosez, and J. Junquera, Highly confined spin-polarized two-dimensional electron gas in SrTiO₃/SrRuO₃ superlattices, *Phys. Rev. Lett.* **108**, 107003 (2012).
- [21] B. Sohn, J. R. Kim, C. H. Kim, S. Lee, S. Hahn, Y. Kim, S. Huh, D. Kim, Y. Kim, W. Kyung *et al.*, Observation of metallic electronic structure in a single-atomic-layer oxide, *Nat. Commun.* **12**, 6171 (2021).
- [22] J. M. Rondinelli, N. M. Caffrey, S. Sanvito, and N. A. Spaldin, Electronic properties of bulk and thin film SrTiO₃: Search for the metal-insulator transition, *Phys. Rev. B* **78**, 155107 (2008).
- [23] Z. Ali, Z. Wang, A. O'Hara, M. Saghayezhian, D. Shin, Y. Zhu, S. T. Pantelides, and J. Zhang, Origin of insulating and non-ferromagnetic SrTiO₃ monolayers, *Phys. Rev. B* **105**, 054429 (2022).
- [24] M. Izumi, K. Nakazawa, and Y. Bando, T_C suppression of SrRuO₃/SrTiO₃ superlattices, *J. Phys. Soc. Jpn.* **67**, 651 (1998).
- [25] N. C. Bristowe, T. Fix, M. G. Blamire, P. B. Littlewood, and E. Artacho, Proposal of a one-dimensional electron gas in the steps at the LaAlO₃-SrTiO₃ interface, *Phys. Rev. Lett.* **108**, 166802 (2012).
- [26] B. Kalisky, E. M. Spanton, H. Noad, J. R. Kirtley, K. C. Nowack, C. Bell, H. K. Sato, M. Hosoda, Y. W. Xie, Y. Hikita *et al.*, Locally enhanced conductivity due to the tetragonal domain structure in LaAlO₃/SrTiO₃ heterointerfaces, *Nat. Mater.* **12**, 1091 (2013).
- [27] S. Smink, H. Boschker, A. Brinkman, J. Mannhart, and H. Hilgenkamp, Capacitive probing of electronic phase separation in an oxide two-dimensional electron system, *Phys. Rev. B* **106**, 054205 (2022).
- [28] H. Boschker, T. Harada, T. Asaba, R. Ashoori, A. V. Boris, H. Hilgenkamp, C. R. Hughes, M. E. Holtz, L. Li, D. A. Muller *et al.*, Ferromagnetism and conductivity in atomically thin SrRuO₃, *Phys. Rev. X* **9**, 011027 (2019).
- [29] F. Gellé, R. Chirita, D. Mertz, M. V. Rastei, A. Dinia, and S. Colis, Guideline to atomically flat TiO₂-terminated SrTiO₃(001) surfaces, *Surf. Sci.* **677**, 39 (2018).
- [30] F. Sánchez, C. Ocal, and J. Fontcuberta, Tailored surfaces of perovskite oxide substrates for conducted growth of thin films, *Chem. Soc. Rev.* **43**, 2272 (2014).